ORIGINAL ARTICLE

Exploring 1, 2, 4-triazole-3-thiol Scaffolds: Design, Synthesis, and Molecular Docking Studies for Tuberculosis Therapy

Suresh Honnalli[1], Soniya Phadte[2], Sagar Shiraguppi[1], Pooja Koganole[1], Sushmita Hiremath[1], Prashant Yuvaraj Mali[3]

[1]Department of Pharmaceutical Chemistry, KLE College of Pharmacy, Vidyanagar, Hubballi, Karnataka, India, [2]Department of Pharmaceutical Chemistry, P.E.S's Rajaram and Tarabai Bandekar College of Pharmacy, Ponda, Goa, India, [3]Department of Pharmacology and Pharmacy Practice, Yashwantrao Bhonsale College of Pharmacy, Sindhudurg, Maharashtra, India

Abstract

Background: Tuberculosis (TB), caused by the pathogen *Mycobacterium tuberculosis*, remains a pressing global health challenge. To design, synthesize, and evaluate novel 1,2,4-triazole-3-thiol derivatives as potential anti-tubercular agents to combat drug-resistant *M. tuberculosis*. **Materials and Methods:** A series of six 1,2,4-triazole-3-thiol derivatives (R1–R6) was rationally designed and synthesised, with structural confirmation by infrared and nuclear magnetic resonance spectroscopy. Molecular docking was performed using AutoDock Vina *via* the PyRx platform against epidermal growth factor receptor kinase (EGFRK; Protein Data Bank ID: 5OEQ). The stability of ligand–protein complexes was assessed using normal mode analysis (NMA) through the iMODS server. Pharmacokinetic and toxicity profiles were predicted using pkCSM, PreADMET, and OSIRIS tools. *In vitro* anti-tubercular activity was evaluated against *M. tuberculosis* H37Rv using the microplate alamar blue assay. **Results and Discussion:** Docking studies identified compound R1 as the most promising candidate, exhibiting the highest binding affinity (−8.1 kcal/moL) with key interactions in the ATP-binding pocket of EGFRK. NMA supported the stability and flexibility of the docked complexes. Absorption, distribution, metabolism, excretion, and toxicity predictions showed that all compounds complied with Lipinski's rule, possessed favorable absorption characteristics, low blood-brain barrier permeability, and minimal predicted toxicity. Biological evaluation revealed that compounds R1, R2, and R4 demonstrated significant anti-tubercular activity, with minimum inhibitory concentrations ranging from 6.25 to 12.5 µg/mL. **Conclusion:** The combined computational and experimental results highlight 1,2,4-triazole-3-thiol derivatives, particularly R1, as promising lead candidates for further development of novel anti-tubercular therapeutics.

Key words: Absorption, distribution, metabolism, excretion, and toxicity, Alamar blue assay, docking, Ramachandran plot, triazole, tuberculosis

INTRODUCTION

Tuberculosis (TB), caused by the pathogen *Mycobacterium tuberculosis*, remains a pressing global health challenge.[1] Despite significant advancements in medical science, TB remains a premier global health threat, accounting for nearly 10% of all infectious disease fatalities.[2] In 2022, the World Health Organization reported a staggering 10.5 million new cases and 1.4 million deaths, with the highest burden concentrated in Asian and African nations.[3] This burden is exacerbated by the dual challenges of TB with human immunodeficiency virus infection and the rise of resistant strains, including multidrug-resistant TB (MDR-TB) and extensively drug-resistant TB (XDR-TB).[4] The inherent

Address for correspondence:
Soniya Phadte, Department of Pharmaceutical Chemistry, P.E.S's Rajaram and TarabaiBandekar College of Pharmacy, Ponda, Goa, India. Mobile: +91-9011969388.
E-mail: snya.nk@gmail.com

Received: 14-02-2026
Revised: 04-05-2026
Accepted: 22-05-2026

resistance of *M. tuberculosis* is largely driven by its unique, lipid-rich cell wall. This dense layer of mycolic acids acts as a formidable physical barrier, shielding the pathogen from antibiotics and ensuring its survival in hostile environments.[5] Furthermore, phenotypic resistance, in which bacteria exhibit reduced susceptibility to antibiotics due to their metabolic state rather than genetic mutations, complicates the combat of TB. "The classification of drug-resistant TB strains, ranging from MDR-TB to XDR-TB, pre-XDR, and total drug-resistant-TB, illustrates the scale and severity of this growing threat."[6-9] While traditional first-line treatments, such as isoniazid and ethionamide, focus on disrupting the Fatty acid synthetase II system to inhibit cell wall synthesis. However, rising resistance has necessitated the search for new enzymatic targets.[10]

The enzyme Decaprenylphospho-β-D-ribofuranose-2′-oxidase (DprE1) has emerged as a vital target. DprE1enzyme and DprE2convert DPR into decaprenylphosphoryl-D-arabinose.[11] It is a critical precursor required for the biosynthesis of arabinan, which is an essential polysaccharide component of the *M. tuberculosis* cell wall. Inhibiting DprE1 effectively halts bacterial growth, making it a highly validated target for drug development.[12,13] 1,2,4-triazoles have gained considerable attention due to their chemical stability and ability to form strong biological bonds through hydrogen bonding π–π stacking.[14] This interactional versatility positions 1,2,4-triazoles as valuable scaffolds in the design of bioactive molecules. Incorporating a thiol (-SH) functional group at the third position of the 1,2,4-triazole ring significantly enhances biological activity. This improvement is due to the group's ability to undergo metal coordination, nucleophilic reactions, and enzyme inhibition mechanisms that are crucial for achieving antimicrobial and anti-tubercular effects.[15] Derivatives of 1,2,4-triazole-3-thiol have shown broad antimicrobial activity, with some achieving potent minimum inhibitory concentrations (MICs) in the range of 1.6–6.25 µg/mL against the virulent *M. tuberculosis* H37Rv strain, by inhibiting critical enzymes involved in the biosynthesis of the *M. tuberculosis* cell wall, such as InhA (enoyl-ACP reductase) and DprE1, suggesting strong potential for therapeutic development.[16-18] Therefore, in the present research authors have planned to design, synthesize, and evaluate novel 1,2,4-triazole-3-thiol derivatives as potential anti-tubercular agents to combat drug-resistant *M. tuberculosis*.

MATERIALS AND METHODS

Chemicals

The chemicals were procured from reputable suppliers, including Sigma-Aldrich, NICE Chemicals, S. D. Fine-Chem Ltd. (Mumbai), and Spectrochem Pvt. Ltd. (Mumbai).

Instruments and equipment's

The melting points of the synthesised compounds were determined using Thiele's melting point apparatus and are reported without correction. Ultraviolet (UV) absorption spectra were recorded on a Shimadzu UV-1900i spectrophotometer. Fourier-transform infrared spectra were obtained using a Shimadzu IR affinity-1 spectrophotometer with the attenuated total reflection technique.^{1}H and ^{13}C nuclear magnetic resonance (NMR) spectra were recorded on a Bruker Avance II 400 MHz spectrometer. Deuterated dimethyl sulfoxide (DMSO-d_6) served as the solvent, and tetramethylsilane was used as the internal standard. Chemical shifts (δ) are reported in parts per million (ppm).

Synthesis

The strategy for the synthesis of substituted 4,5-diphenyl-4*H*-1,2,4-triazole-3-thiol derivatives R1–R6 is described in Figure 1.

Synthesis of substituted methylbenzoate II a-f

Substituted benzoic acid (0.1 moL) was subjected to esterification by refluxing with concentrated sulfuric acid (2 mL, 98.079 g/moL) in 150 mL of methanol. The reaction mixture was continuously stirred and maintained at 80–90°C for 18–20 h. On completion of the reaction, the solid or oily liquid ester was cooled to room temperature and poured over crushed ice to induce product precipitation. The resulting product was then separated by filtration. The progress and completion of the reaction were monitored by thin-layer chromatography (TLC) using ethyl acetate and hexane in a 1:4 ratio as the mobile phase.[19]

Synthesis of methyl-4-nitrobenzoate IIa

White solid, M.P.: 98–96°C, Yield (%): 93%, Molecular formula- $C_8H_7NO_4$, Molecular weight- 181.15 g/moL. IR (KBr, cm^{-1}): 3086.19 (Ar. C-H), 1784.95 (C=O), 1541.46 Asymm. (NO_2), 1324.14 Symm. (NO_2). ^{1}HNMR (DMSO, δ ppm): 8.17 (d,2H,CH [NO_2]), 7.89 (d,2H,CH), 3.49 (s,3H, CH_3).

Synthesis of methyl-2-fluorobenzoate IIb

Colorless solid, M.P: 94–92°C, Yield (%): 67%, Molecular formula- $C_8H_7FO_2$, Molecular weight- 154.14 g/moL. IR (KBr, cm^{-1}): 3086.57 (Ar. C-H), 1778.15 (C=O), 1203.56 (C-F). ^{1}HNMR (DMSO, δ ppm): 8.17 (d,1H,CH(C6)), 7.89 (t,1H,CH(C4)), 7.35 (d,1H, CH(C3)), 7.23 (t,1H,CH(C5)), 3.89 (s,3H, CH_3).

Synthesis of methyl-3,4,5-trimethoxybenzoate IIc

Off-white solid, M.P.: 80–78°C, Yield (%): 73%, Molecular formula- $C_{11}H_{14}O_5$, Molecular weight- 226.23 g/moL. IR (KBr, cm^{-1}): 3034.76 (Ar. C-H), 1759.23 (C=O), 1305.45 (C-O-C). ^{1}HNMR (DMSO, δ ppm): 7.19 (s,2H,Ar.CH), 3.89 (s,3H,$COOCH_3$), 3.19 (s,9H,OCH_3).

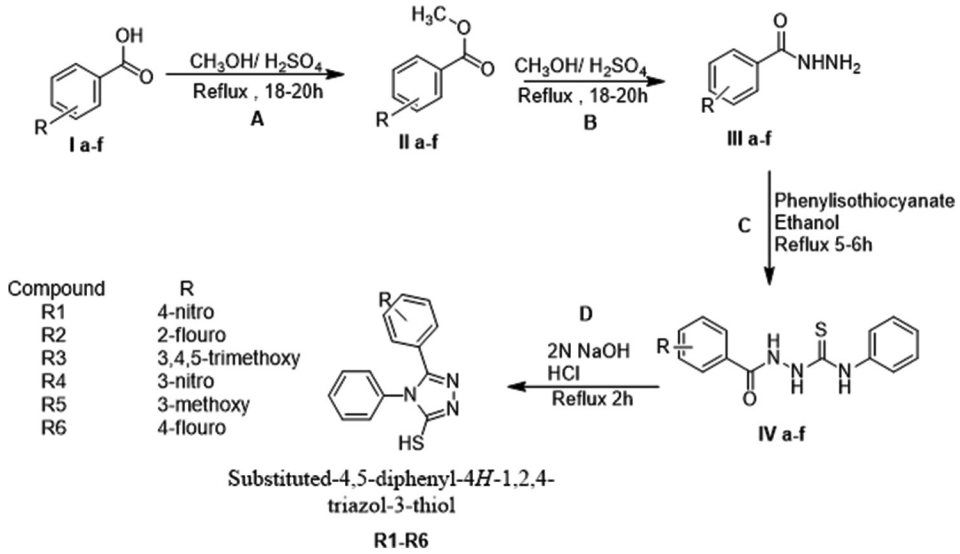

Figure 1: Synthesis of substituted -4,5-diphenyl-4H-1,2,4-triazol-3-thiol derivatives

Synthesis of methyl-3-nitrobenzoate IId

Light yellow solid, M.P.: 80–78°C, Yield (%): 81%, Molecular formula- $C_8H_7NO_4$, Molecular weight- 181.15 g/moL. IR (KBr, cm^{-1}): 3056.84 (Ar. C-H), 1755.67 (C=O), 1554.65 (Assym. NO_2), 1342.74 (Symm. NO_2), 1294.56 (C-O-C).[1] HNMR (DMSO, δ ppm):8.60 (s,1H,Ar.CH), 8.47 (d,1H, Ar.CH), 8.44 (d,1H,Ar.CH), 7.82 (t,1H, Ar.CH), 3.29 (s,3H,OCH_3).

Synthesis of methyl-3-methoxybenzoate IIe

White solid, M.P.: 48–46°C, Yield (%): 72%, Molecular formula- $C_9H_{10}O_3$, Molecular weight- 166.15 g/moL. IR (KBr, cm^{-1}): 3023.41 (Ar. C-H), 1762.84 (C=O), 1203.45 (C-O-C).[1] HNMR (DMSO, δ ppm):7.75 (t,1H,Ar.CH), 7.60 (s,1H, Ar.CH), 7.61 (d,1H,Ar.CH), 7.20 (d,1H, Ar.CH), 3.83 (s,3H,$COOCH_3$), 3.29 (s,3H,OCH_3).

Synthesis of methyl-4-fluorobenzoate IIf

Light yellow liquid, M.P.: 92–90°C, Yield (%): 56%, Molecular formula- $C_8H_7FO_2$, Molecular weight- 154.14 g/moL.IR (KBr, cm^{-1}): 3072.16 (Ar. C-H), 1764.34 (C=O), 1362.74 (C-F), 1203.45 (C-O-C).[1]HNMR (DMSO, δ ppm): 8.82 (d,2H,Ar.CH), 7.73 (d,2H, Ar.CH), 3.13 (s,3H,OCH_3).

Synthesis of substituted benzohydrazide III a-f

Substituted methylbenzoate (0.1 moL) was reacted with hydrazine hydrate (0.5 moL, 50 g/moL) in a 1:5 molar ratio using methanol as the reaction medium. The mixture was refluxed at a temperature of 80–90°C for 18–20 h under continuous stirring. After completion of the reaction, the reaction mixture was cooled to room temperature and poured onto crushed ice to precipitate the product. The resulting solid was collected by filtration and dried. The progress of the reaction was monitored by TLC using a solvent system of acetone: hexane (6:4) as the mobile phase.[19]

Synthesis of 4-nitrobenzohydrazide (IIIa)

Light Yellow solid, M.P.: 210–205°C, Yield (%): 93%, Molecular formula- $C_7H_7N_3O_3$, Molecular weight- 181.15 g/moL. IR (KBr, cm^{-1}): 3286.09 (N-H), 1666.67 (C=O), 1592.89 (C=C), 1543.23 Asymm. (NO_2), 1342.34 Symm. (NO_2), 1272.56 (C-N).[1] HNMR (DMSO, δ ppm): 9.64 (s,1H, NH), 8.37 (d,2H,CH (NO_2)), 8.15 (d,2H,CH), 2.49 (d,2H, NH_2).

Synthesis of 2-fluorobenzohydrazide (IIIb)

White solid, M.P.: 140–135°C, Yield (%): 82%, Molecular formula- $C_7H_7FN_2O$, Molecular weight- 154.14 g/moL. IR (KBr, cm^{-1}): 3299.78 (N-H), 1642.54 (C=O), 1492.83 Ar. (C=C), 1272.56 (C-N),1222.51 (C-F). [1]HNMR (DMSO, δ ppm): 9.81 (s,1H, NH),7.73 (s,1H, CH), 7.64 (s,1H, CH),7.54 (s,1H, CH),7.40 (s,1H,CH), 2.69 (d,2H, NH_2).

Synthesis of 3,4,5-trimethoxybenzohydrazide (IIIc)

White solid, M.P.: 190–185°C, Yield (%): 89%, Molecular formula- $C_{10}H_{14}N_2O_4$, Molecular weight- 226.23 g/moL. IR (KBr, cm^{-1}):3269.63 (N-H), 2926.85 (Ali.C-H), 1655.45 (C=O), 1272.57 (C-N), 1258 (C-O-C), 1222.34 (C-F). [1]HNMR (DMSO, δ ppm): 9.81 (s,1H,NH), 7.17 (d,2H, CH), 3.83 (s, 9H, CH_3), 2.74 (d,2H, NH_2).

Synthesis of 3-nitrobenzohydrazide (IIId)

Light Yellow solid, M.P.: 210–205°C, Yield (%): 93%, Molecular formula- $C_7H_7N_3O_3$, Molecular weight- 181.15 g/moL. IR (KBr, cm^{-1}): 3269.34 (N-H), 1626.78 (C=O), 1582.49Ar (C=C), 1529.83Asymm. (NO_2), 1315. 48Symm (NO_2), 1272.38 (C-N).[1] HNMR (DMSO, δ ppm): 9.97 (s,1H,NH), 8.72 (s,1H,CH), 8.46 (s,1H,CH),8.34 (s,1H,CH), 7.85 (s,1H,CH), 2.89 (d,2H,NH_2).

Synthesis of 3-methoxybenzohydrazide (IIIe)

White solid, M.P.: 165–160°C, Yield (%): 79%, Molecular formula- $C_8H_{10}N_2O_2$, Molecular weight- 166.18 g/moL. IR

(KBr, cm^{-1}): 3272.67 (N-H), 2910.28 (Ali. C-H), 1675.45 (C=O), 1272.56 (C-N), 1269.41 (C-O-C) ^{1}HNMR (DMSO, δ ppm): 9.81 (s,1H, NH), 7.71 (s,1H, CH),7.63 (s,1H, CH), 7.19 (s,1H, CH),6.77 (s,1H, CH), 3.77 (s, 3H,CH_3), 2.74 (d,2H, NH_2).

Synthesis of 4-fluorobenzohydrazide (IIIf)

White solid, M.P.: 149–145°C, Yield (%): 82%, Molecular formula- $C_7H_7FN_2O$, Molecular weight- 154.14 g/moL. IR (KBr, cm^{-1}): 3289.73 (N-H), 1639.58 (C=O), 1256.93 (C-N), 1232.38 (C-F). ^{1}HNMR (DMSO, δ ppm): 9.64 (s,1H, NH), 8.12 (d,2H, CH), 7.37 (d,2H, CH), 3.49 (d,2H, NH_2).

Synthesis of substituted 2-benzoyl-N-phenylhydrazinecarbothioamide IV a-f

Benzoic acid hydrazide (10 mmoL) was reacted with phenylisothiocyanate (15 mmoL) in ethanol under reflux conditions for 4 h. On completion, the reaction mixture was allowed to cool to room temperature, leading to the formation of a white solid precipitate. The solid was collected by filtration and purified by recrystallization from ethanol to obtain the desired product.[20]

Synthesis of 2-(4-nitrobenzoyl)-N-phenylhydrazine-1-carbothioamide (IVa)

Yellow solid, M.P.: 210–206°C, Yield (%): 91%, Molecular formula- $C_{14}H_{12}N_4O_3S$, Molecular weight- 316.34 g/moL. IR (KBr, cm^{-1}): 3332.38 (N-H), 3092.67Ar (C-H), 1686.42 (C=O), 1523.43 Asymm. (NO_2), 1352.45Symm (NO_2), 1232.31 (C=S). ^{1}HNMR (DMSO, δ ppm): 10.74 (s,1H, NH), 8.37 (d,2H,CH), 8.15 (d,2H,CH), 7.07 (d,2H,CH), 6.73 (t,2H,CH), 6.69 (t,1H, CH), 4.25 (s,1H,NH), 3.51 (s,1H, NH).

Synthesis of 2-(2-fluorobenzoyl)-N-phenylhydrazine-1-carbothioamide (IVb)

Cream white solid, M.P.: 198–196°C, Yield (%): 88%, Molecular formula- $C_{14}H_{12}FN_3OS$, Molecular weight- 289.33 g/moL. IR (KBr, cm^{-1}): 3362.98 (N-H), 3056.45Ar. (C-H), 1666.57 (C=O), 1225.39 (C=F), 1245.63 (C=S). ^{1}HNMR (DMSO, δ ppm): 10.45 (s,1H,NH), 8.35 (d,1H,CH), 8.14 (t,1H,CH), 7.51 (d,1H,CH), 7.29 (t,1H,CH), 7.15 (d,1H,ph. CH), 7.07 (t,2H,ph. CH), 6.73 (t,1H,ph.CH), 4.67 (s,1H,NH), 3.51 (s,1H,NH).

Synthesis of 2-(3,4,5-trimethoxybenzoyl)-N-phenylhydrazine-1-carbothioamide (IVc)

Off whitish solid, M.P.: 202–200°C, Yield (%): 88%, Molecular formula- $C_{17}H_{19}N_3O_4S$, Molecular weight- 361.42 g/moL. IR (KBr, cm^{-1}): 3292.86 (N-H stretch), 3064.57 (Ar. C-H), 1689 (C=O), 1345.39 (C-O-C), 1208 C=S. ^{1}HNMR (DMSO, δ ppm): 11.32 (s,1H, NH), 7.70 (s,2H, CH), 7.43 (d,2H, ph.CH), 7.17 (t,2H, ph.CH), 7.09 (t,1H, ph.CH), 4.67 (s,1H, N-H), 3.84 (s,1H,N-H), 3.71 (s,9H,CH_3).

Synthesis of 2-(3-nitroybenzoyl)-N-phenylhydrazine-1-carbothioamide (IVd)

Light yellowish solid, M.P.: 185–191°C, Yield (%): 96%, Molecular formula- $C_{14}H_{12}N_4O_3S$, Molecular weight- 316.34 g/moL. IR (KBr, cm^{-1}): 3302.89 (N-H), 3052.41 Ar.(C-H), 1679.39 (C=O), 1529.83Asymm. (NO_2), 1360.65Symm (NO_2), 1238.63 (C=S). ^{1}HNMR (DMSO, δ ppm): 11.32 (s,1H, NH), 8.72 (s,1H, CH), 8.46 (d,1H, CH), 8.35 (d,1H, CH), 7.94 (t,1H,CH), 7.85 (d,2H,ph.CH), 7.70 (t,2H,ph.CH), 7.43 (t,1H,ph.CH), 4.62 (s,1H,N-H), 2.37 (s,1H, N-H).

Synthesis of 2-(3-methoxybenzoyl)-N-phenylhydrazine-1-carbothioamide (IVe)

Pale yellow solid, M.P.: 185–180°C, Yield (%): 92%, Molecular formula- $C_{15}H_{15}N_3O_2S$, Molecular weight: 301.37 g/moL. IR (KBr, cm^{-1}): 3286.58 (N-H), 3032.63Ar. (C-H), 1665.57 (C=O), 1248 (C=S).^{1}HNMR (DMSO, δ ppm): 11.32 (s,1H,NH), 7.71 (t,1H,CH), 7.70 (d,1H,CH), 7.63 (d,1H,CH), 7.43 (s,1H,CH), 7.19 (d,2H,ph.CH), 7.09 (t,2H, ph.CH), 6.77 (t,1H,ph.CH), 4.62 (s,1H,N-H), 3.56 (s,3H,CH_3), 2.77 (s,1H,N-H).

Synthesis of 2-(4-fluorobenzoyl)-N-phenylhydrazine-1-carbothioamide (IVf)

Creamish white solid, M.P.: 179–176°C, Yield (%): 88%, Molecular formula- $C_{14}H_{12}FN_3OS$, Molecular weight- 289.33 g/moL.IR (KBr, cm^{-1}): 3298.45 (N-H), 3069.38 (Ar. CH), 1652.38 (C=O), 1239.62 (C=S), 1196.53 (C-F).^{1}HNMR (DMSO, δ ppm): 11.32 (s,1H, NH), 8.35 (d,2H, CH), 8.12 (d,2H, CH), 7.70 (d,2H, ph.CH), 7.43 (t,2H,CH), 7.37 (s,1H,CH), 4.26 (s,1H, NH), 2.38 (s,1H,NH).

Synthesis of substituted 4,5-diphenyl-4H-1,2,4-triazol-3-thiol derivatives (R1–R6)

Substituted thiosemicarbazide derivatives were treated with 2N sodium hydroxide and subjected to reflux at 100–110°C for 3 h. Following completion of the reaction, the mixture was cooled to room temperature and gradually acidified to a pH of 3–4 using concentrated hydrochloric acid (37%). The resulting precipitate was collected by filtration, thoroughly washed with distilled water, and purified by recrystallization from an ethanol-water mixture (1:1) to yield the cyclized product.[20,21]

Synthesis of 5-(4-nitrophenyl)-4-phenyl-4H-1,2,4-triazole-3-thiol (R1)

Amorphous yellow solid, M.P.: 210–205°C;Yield (%): 97%; Molecular formula: $C_{14}H_{10}O_2N_4S$; Molecular weight: 298.32g/moL.IR (KBr, cm^{-1})**:** 3092.17 (Ar. C-H), 2738.77 (S-H), 1695.81 (C=C), 1598.65 (C=N), 1520.56 (NO_2asymm.) and 1340 (NO_2symm.), 1322.99 (C-N), 694.33 (C-S). ^{1}H-NMR (DMSO, δ ppm): 11.2 (s,1H,SH), 8.16 (d, 2H, J=8.9Hz, NO_2-Ph. H), 7.52 (d,2H,J=8.9Hz, triazole-Ph. H), 7.40-7.20 (m,5H,Ar.-H).^{13}CNMR (DMSO-*d6*, δ ppm): 168.5 (1C, C-SH), 156.7 (1C, C-triazole); 148.3 (1C, C-NO_2), 146.2 (1C, N-C Ph.); 142.9 (1C, C of NO_2-Ph), 128.4-124.3 (9C, Ar.C). Elemental analysis; calculated: C, 56.37; H, 3.38; N, 18.78; O, 10.73; S, 10.75 found: C, 56.17; H, 3.33; N, 18.02; O, 10.15; S, 10.24.

Synthesis of 5-(2-flourophenyl)-4-phenyl-4H-1,2,4-triazole-3-thiol (R2)

Amorphous dark yellow solid, M.P.: 194–190°C; Yield (%): 88%; Molecular formula: $C_{14}H_{10}FN_3S$; Molecular weight: 271.31g/moL. IR (KBr, cm^{-1}):3024.67 (Ar. C-H), 2781.59 (S-H), 1674.87 (C=C), 1585.81 (C=N), 1238.64 (C-F), 1020.89 (C-N), 694.33 (C-S). ^{1}H-NMR ($CDCl_3$, δ ppm): 14.13 (s, 1H, SH), 7.53 (1H,d, H-3', J=8Hz), 7.49 (1H, t,H-4',J=8Hz), 7.37 (1H,d,H-6',J=8Hz), 7.15 (1H, t,H-3',J=8Hz), 7.02-6.89 (5H,m,Ar-H). ^{13}CNMR (DMSO-*d6*, δ ppm): 173.5 (1C, C-SH), 157.4 (1C, C-F), 154.2 (1C, C-triazole); 141.4 (1C, N-C Ph.); 130.1-122.5 (10C, Ar.C). Elemental analysis; calculated: C, 61.98; H, 3.72; F, 7.00; N, 15.49; S, 11.82 found: C, 60.34; H, 3.70; F, 6.56; N, 15.41; S, 11.24.

Synthesis of 5-(3,4,5-trimethoxyphenyl)-4-phenyl-4H-1,2,4-triazole-3-thiol (R3)

Amorphous brown solid, M.P.: 198-194°C; Yield (%): 93%; Molecular formula: $C_{17}H_{17}N_3O_3S$; Molecular weight: 343.30g/mol. IR (KBr, cm^{-1}): 3067.89 (Ar. C-H), 2768.45 (S-H), 1694.78 (C=C), 1578.56 (C=N), 1322.99 (C-N), 1032.57 (C-O-C), 694.33 (C-S). ^{1}H-NMR ($CDCl_3$, δ ppm): 12.22 (s, 1H, SH), 7.02-6.89 (m, 5H, Ar-H), 6.54 (s, 2H, H-2', J=8Hz), 3.59 (s, 9H, O-CH_3). ^{13}CNMR (DMSO-*d6*, δ ppm): 167.4 (1C, C-SH), 152.7 (1C, C-triazole); 143.6 (1C, C-NO_2); 141.2 (1C, N-C Ph.); 127.4-102.4 (8C, Ar.C); 60.7 (3C, CH_3). Elemental analysis; calculated: C, 59.46; H, 4.99; N, 12.24; O, 13.98; S, 9.34 found: C, 59.30, H, 4.14; N, 12.05; O, 13.16; S, 9.24.

Synthesis of 5-(3-nitrophenyl)-4-phenyl-4H-1,2,4-triazole-3-thiol (R4)

Amorphous orange solid, M.P.: 178–174°C; Yield (%): 69%; Molecular formula: $C_{14}H_{10}O_2N_4S$; Molecular weight: 298.32g/mol. IR (KBr, cm^{-1}): 3192.17 (Ar. C-H), 2756.23 (S-H), 1692.56 (C=C), 1593.54 (C=N), 1530.12 (NO_2asymm.) and 1356.78 (NO_2symm.), 1345.67 (C-N), 676.88 (C-S). ^{1}H-NMR (CDCl3, δ ppm): 11.99 (s, 1H, SH), 8.10 (d,1H,J=7.5Hz, H-2' (NO_2-Ph),7.57 (d,1H, H-4', J=7.5 Hz), 7.27 (t,1H,H-5', J=7.5 Hz), 7.20 (d,1H,H-6'), 7.10-6.60 (m,5H,Ph-H).^{13}CNMR (DMSO-*d6*, δ ppm): 168.5 (1C, C-SH), 156.7 (1C, C-triazole); 148.3 (1C, C-NO_2), 146.2 (1C, N-C Ph.); 141.0 (1C, C of NO_2-Ph), 130.6-121.9 (9C, Ar.C). Elemental analysis; calculated: C, 56.37; H, 3.38; N, 18.78; O, 10.73; S, 10.75 found: C, 56.04; H, 3.17; N, 18.46; O, 10.05; S, 10.35.

Synthesis of 5-(3-methoxyphenyl)-4-phenyl-4H-1,2,4-triazole-3-thiol (R5)

Amorphous light yellow solid, M.P.: 192–190°C; Yield (%): 69%; Molecular formula: $C_{15}H_{13}ON_3S$; Molecular weight: 283.34g/moL IR (KBr, cm^{-1}): 3024.95 (Ar. C-H), 2712.65 (S-H), 1667.45 (C=C), 1523.56 (C=N), 1334.45 (C-N), 1205.67 (C-O-C), 694.33 (C-S). ^{1}H-NMR (DMSO, δ ppm):14.12 (s, 1H, SH), 7.84 (s, 1H, H-6'), 7.58-7.45 (m, 5H, Ar.H), 7.36 (s, 1H, H-2'), 7.24 (s, 1H, H-5'), 7.08 (s, 1H, H-4'), 3.58 (s, 3H, O-CH_3). ^{13}CNMR (DMSO-*d6*, δ ppm): 172.3 (1C, C-SH), 161.6 (1C, OCH_3), 154.2(1C, C-triazole), 142.7 (1C, N-C Ph.); 131.9-125.6 (10C, Ar.C); 53.9 (1C, CH_3). Elemental analysis; calculated: C, 63.58; H, 4.62; N, 14.83; O, 5.65; S, 11.32 found: C, 62.92; H, 4.16; N, 14.30; O, 5.34; S, 11.03.

Synthesis of 5-(4-flourophenyl)-4-phenyl-4H-1,2,4-triazole-3-thiol (R6)

Amorphous dark brown solid, M.P.: 184–180°C; Yield (%):70%; Molecular formula: $C_{14}H_{10}F\ N_3S$; Molecular weight: 271.31 g/moL. IR (KBr, cm^{-1}): 3078.94 (Ar. C-H), 2745.77 (S-H), 1693.45 (C=C), 1590.34 (C=N), 1312.56 (C-N), 1187.56 (C-F), 692.56 (C-S). ^{1}H-NMR (CDCl3, δ ppm): 14.13 (s, 1H, SH), 7.52 (2H,d, F-Ph.H,J=8Hz), 7.49 (1H,d,triazole-Ph.H,J=8Hz), 7.27–6.39 (m, 5H, Ar-H). ^{13}CNMR (DMSO-*d6*, δ ppm): 167.4 (1C, C-SH), 161.9 (1C, C-F), 150.9 (1C, C-triazole); 141.2 (1C, N-C Ph.); 130.3-116.4 (10C, Ar.C). Elemental analysis; calculated: C, 61.98; H, 3.72; F, 7.00; N, 15.49; S, 11.82 found: C, 61.13; H, 3.45; F, 6.94; N, 15.17; S, 11.11.

Computational analysis

Ramachandran plot analysis and structure validation of protein

The stereochemical quality of the modeled protein structure, epidermal growth factor receptor kinase with Protein Data Bank (PDB) ID 5OEQ, was evaluated using the Procheck web server, which comprehensively assesses structural geometry through various validation parameters, including the Ramachandran plot. The protein structure file obtained post-modeling was submitted to Procheck in PDB format. The Ramachandran plot was generated to analyse the distribution of backbone dihedral angles (phi ϕ and psi ψ) for each amino acid residue, excluding glycine (GLY) and proline (PRO) due to their atypical conformational flexibility. The residues were categorized into most favored, additionally allowed, generously allowed, and disallowed regions based on established steric criteria. Additional procheck outputs were used to evaluate bond lengths, bond angles, planarity of peptide bonds, chi1-chi2 side-chain conformations, and overall G-factors, which indicate the geometric and conformational quality of the model. The presence of any bad contacts or cis-peptides was also recorded to identify possible structural anomalies. The results provided insight into the modeled protein's overall stereochemical reliability and suitability for further computational studies.[22,23]

Molecular docking procedure using PyRx and AutoDock

Molecular docking studies were performed to evaluate the binding interactions of the synthesised compounds (R1–R6) with the target protein using PyRx10 virtual screening software, which integrates AutoDockVina for docking operations. The crystal structure of the EGFR

kinase domain (PDB ID: 5OEQ) was retrieved from the RCSB PDB and prepared by eliminating water molecules, co-crystallized ligands, and ions. Hydrogen atoms were added, and appropriate charges were assigned using AutoDock Tools, and the final structure was saved in PDBQT format for docking studies. The 2D structures of the test compounds were drawn in ChemDraw and converted into 3D conformations using Open Babel within PyRx 10. These structures were subjected to energy minimization using the Universal Force Field to obtain stable conformations, and subsequently saved in PDBQT format. Docking was performed by defining a grid box that covered the active site region, based on reported residues and the co-crystallized ligand. AutoDockVina, integrated into PyRx 10, was employed for docking using default parameters. The docked complexes were evaluated based on binding affinity and binding orientation. The most stable poses were selected and analysed for key interactions such as hydrogen bonds and hydrophobic contacts using Discovery Studio Visualizer and PyMOL.[24-26]

In silico molecular docking and simulation studies

To investigate the structural flexibility and dynamic stability of the docked complex involving PDB ID: 5OEQ, normal mode analysis (NMA) was performed using the iMODS web server (https://imods.iqfr.csic.es/). The crystal structure of PDB ID: 5OEQ, representing the target protein, was retrieved from the RCSB PDB and subjected to docking studies with the designed ligand. The resulting protein–ligand complex in PDB format was used as input for iMODS. The analysis included an assessment of deformability, eigenvalues, B-factor predictions, variance, and covariance matrices to predict the complex's flexibility. Deformability graphs indicated the mobility of each residue, while eigenvalues reflected the energy required to deform the structure; lower eigenvalues correspond to greater structural flexibility. The variance associated with each normal mode was calculated, with higher variances signifying more significant conformational fluctuations. The covariance matrix depicted correlated (red), anti-correlated (blue), and uncorrelated (white) movements among residues, which aided in identifying potential flexible or rigid regions within the complex. Elastic network models were also generated to visualize the strength and extent of interatomic interactions. The comprehensive iMODS-based analysis enabled the understanding of the dynamic stability of the six ligand-protein complexes under physiological conditions, supporting its potential as a viable therapeutic candidate.[27-29]

In silico absorption, distribution, metabolism, excretion, and toxicity (ADMET) studies and drug likeliness

The *in silico* assessment of pharmacokinetic and drug-likeness properties of the synthesised compounds was performed using various web-based predictive platforms. Drug-likeness was analysed through the PreADME, OSIRIS Property Explorer, and pkCSM servers, applying commonly accepted filters such as Lipinski's Rule of Five, along with Ghose, Veber, Egan, and Muegge criteria to evaluate oral bioavailability, physicochemical compatibility, and structural drug-likeness.[30-34] The pkCSM tool was further employed to estimate ADMET parameters, providing insights into the compounds' pharmacokinetic behavior. Toxicological profiles, including LD_{50} values and organ-specific toxicity predictions, were determined using the ProTox-II web server, which uses machine learning algorithms based on chemical structure. This integrative computational approach enabled a comprehensive theoretical evaluation of the compounds' suitability as drug candidates.[35]

Biological activity

The synthesised 4,5-diphenyl-4*H*-1,2,4-triazole-3-thiol derivatives R1–R6 were tested for their antitubercular activity against *M. tuberculosis* H_3RV using the microplate alamar blue assay (MABA) method. The study was carried out by using standard drugs like isoniazid and rifampicin.[36]

Anti-mycobacterial assay protocol

A fresh culture grown on Lowenstein-Jensen medium was used to prepare the inoculum, which was re-suspended in Middlebrook 7H9-S broth supplemented with 0.1% casitone, 0.5% glycerol, and oleic acid, albumin, dextrose, and catalase. The suspension was adjusted to McFarland standard No. 1 and further diluted (1:20), and 100 µL was used to inoculate each well. Test compounds were dissolved in DMSO, with vehicle controls included to account for solvent effects. The final DMSO concentration in all wells was maintained below 0.5% (v/v), ensuring no interference with mycobacterial growth. Stock solutions of the test compounds were thawed and diluted in 7H9-S to a concentration four times higher than the maximum final test concentration. Two-fold serial dilutions were performed directly in sterile 96-well microtiter plates, resulting in final test concentrations of 100, 50, 25, 12.5, and 6.25 µg/mL. Peripheral wells were filled with sterile deionized water to reduce evaporation during incubation. Each assay plate includes a growth control (medium with inoculum but without compound) and a sterility control (medium without inoculum or compound). Plates were covered, sealed in plastic bags, and incubated at 37°C under aerobic conditions, then sealed and incubated at 37°C under aerobic conditions. After 7 days, Alamar Blue reagent was added, and plates were incubated overnight. A color change from blue to pink indicated bacterial growth. The MIC was determined as the lowest concentration that prevented this color change and was expressed in µg/mL.

RESULTS AND DISCUSSION

Comprehensive stereochemical validation of the modeled protein using ProCheck and Ramachandran plot analysis

The structural validation of the modeled protein EGFRK was carried out using the PROCHECK tool, emphasising the Ramachandran plot to evaluate backbone dihedral angle distributions as shown in Figure 2. The plot revealed that 92.8% of the residues were located within the most favored regions [A, B, L], indicating a well-folded and conformationally stable protein structure. Furthermore, 7.1% of residues occupied additional allowed regions, while only 0.1% were found in generously allowed regions. Importantly, no residues were observed in disallowed regions, signifying excellent stereochemical integrity with minimal steric strain or conformational outliers. Among the 843 total residues, 707 were non-GLY and non-PRO residues, while 85 GLY and 42 PRO residues were also present. GLY residues, represented as triangles in the plot due to their enhanced torsional flexibility, and PRO residues, which have restricted phi angles, were appropriately distributed. Side-chain parameter evaluation showed that five residues exhibited improved conformations, whereas eight residues were flagged in Chi1-Chi2 plots (from a total of 409), likely corresponding to flexible or solvent-accessible regions.

Further structural assessments reinforced the model's reliability. Bond length and angle deviations remained within acceptable thresholds, with a maximum deviation of 4.7 and a bond geometry standard deviation of 4.0. G-factor values were −0.24 for dihedral angles, 0.37 for covalent geometry, and 0.01 overall, all within recommended limits, supporting the plausibility of the model's geometric configuration. In addition, 100% of the planar groups were within acceptable parameters, and only a single bad contact was identified, underscoring the overall quality of the protein model. Two

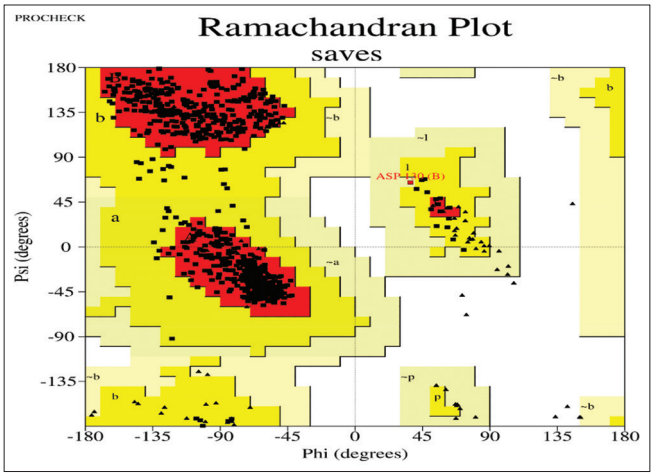

Figure 2: Ramachandran plot analysis of the epidermal growth factor receptor kinase modeled protein structure using PROCHECK

cis-peptides were also detected, which may reflect biologically relevant structural features or require further validation. The PROCHECK validation results and Ramachandran plot statistics confirm the high quality of the predicted protein structure. The absence of disallowed residues, coupled with favorable stereochemistry, suggests that the EGFRK model is well-suited for downstream computational studies such as molecular docking, virtual screening, and molecular dynamics simulations.

Molecular interaction analysis of synthesised compounds (R1–R6)

Molecular docking studies were performed to evaluate the binding affinity and interaction profiles of a series of synthesized thiosemicarbazide derivatives (R1–R6) with the EGFRK enzyme crystal structure (PDB ID: 5OEQ), and the results are tabulated in Table 1. These compounds were docked into the ATP-binding site of the receptor to gain insights into their potential inhibitory activity, as depicted in Figure 3. Compound R1 exhibited a docking score of -8.4 kcal/mol and established two key hydrogen bonds with Glutamine-788 and Glutamate-762. These polar interactions were supported by additional π-alkyl contacts with Cysteine (CYS)-797, Valine (VAL)-726, and Leucine (LEU)-844, indicating a well-positioned and stabilised binding conformation within the hydrophobic pocket. The 3D structures of the binding interaction of R1 with the binding site of EGFRK are shown in Figure 4. Compound R2, with a docking score of −7.7 kcal/mol, had hydrophobic interactions with residues Alanine (ALA)-743, VAL-726, ALA-751, and Arginine (ARG)-841. Although it lacked hydrogen bonds, the ligand maintained a stable orientation within the binding site. Compound R3 showed a docking score of −7.7 kcal/mol and formed two hydrogen bonds with Aspartate (ASP)-855 and Asparagine -842, both located in the hinge region of EGFRK. The compound also exhibited π-alkyl interactions with ALA-743 and ARG-841, contributing to a balanced polar and non-polar interaction profile. Compound R4 displayed a docking score of −7.6 kcal/mol, forming a hydrogen bond with GLY-719 at the active site, and hydrophobic interactions with CYS-797, VAL-726, and ALA-743. The presence of a polar substituent in this compound might have enhanced its electrostatic binding with the receptor at the binding pocket.

Compound R5 demonstrated a docking score of −7.7 kcal/mol. It exhibited dual hydrogen bonding with GLY-719 and ASP-855, anchoring it effectively within the kinase hinge region. Further stabilization was achieved through hydrophobic interactions with ALA-743 and ARG-841. R6exhibited a docking score of −7.5 kcal/moL, forming hydrogen bonds with GLY-719 and ASP-855, and hydrophobic interactions with PRO-794, VAL-726, and ARG-841. Collectively, the docking results confirm that all six derivatives possess the ability to interact efficiently with the EGFR kinase active site. Compound R1, in particular,

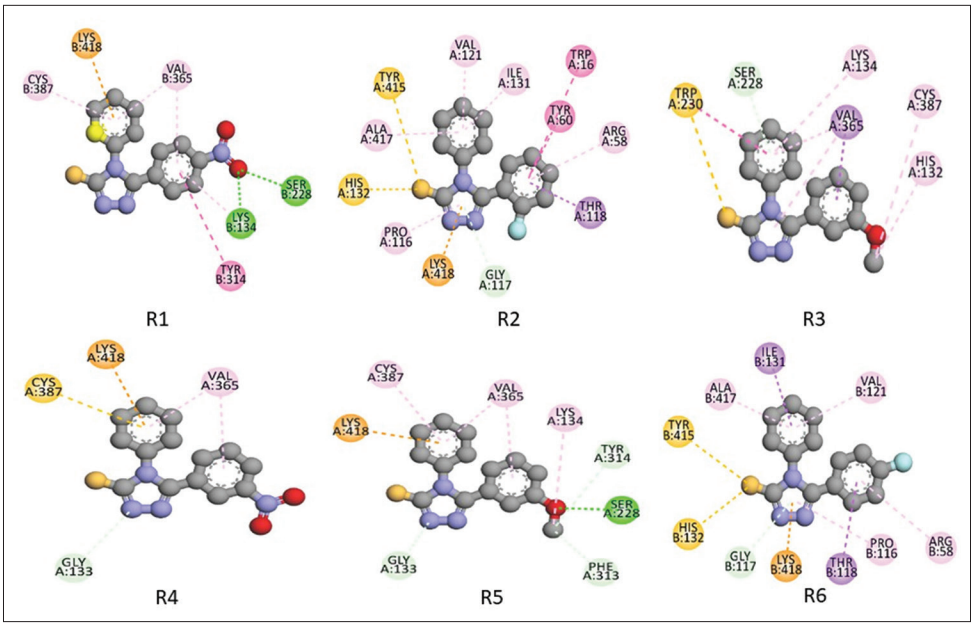

Figure 3: 2D structures of docking Interactions of synthesized thiosemicarbazide derivatives (R1–R6) with epidermal growth factor receptor kinase (Protein Data Bank ID: 5OEQ)

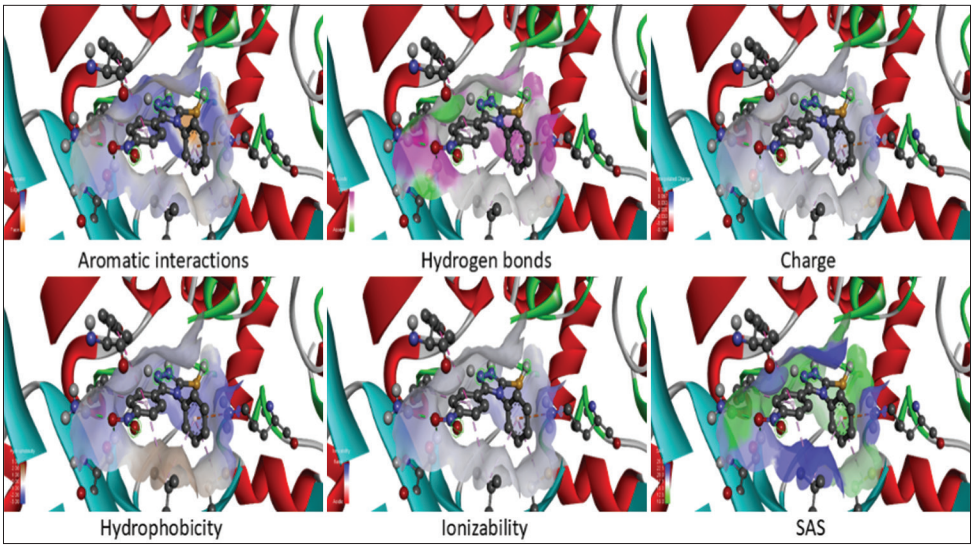

Figure 4: 3D binding interactions of R1 with key residues of epidermal growth factor receptor kinase enzyme (Protein Data Bank ID: 5OEQ)

exhibited superior binding energies and showed both hydrogen bonding and hydrophobic contacts, positioning it as a promising candidate for further biological evaluation as a potential EGFRK inhibitor.

Structural flexibility and dynamic stability of PDB ID: 5OEQ and synthesised ligand complexes

NMA using the iMODS web server was performed to evaluate the dynamic behavior and structural flexibility of protein–ligand complexes involving PDB ID: 5OEQ and six 1,2,4-triazole-based ligands (R1–R6), Figure 5. Among them, R1 [5-(4-nitrophenyl)-4-phenyl-4H-1,2,4-triazole-3-thiol] showed the highest binding affinity (–8.1 kcal/mol) and the most favorable dynamic profile. Its B-factor analysis indicated low atomic mobility near the binding site, while the deformability plot showed minimal peaks at terminal regions, suggesting a stable complex. A moderate eigenvalue reflected a balance between flexibility and stability, and the covariance map demonstrated correlated domain motions. The dense elastic network further indicated strong interatomic interactions, highlighting R1 as the most promising candidate.

Compounds R2, R3, and R5 (–7.7 kcal/moL) also exhibited low B-factors and deformability, although R3 showed slightly higher peripheral flexibility. Their eigenvalue and variance profiles supported functional motion with maintained stability.

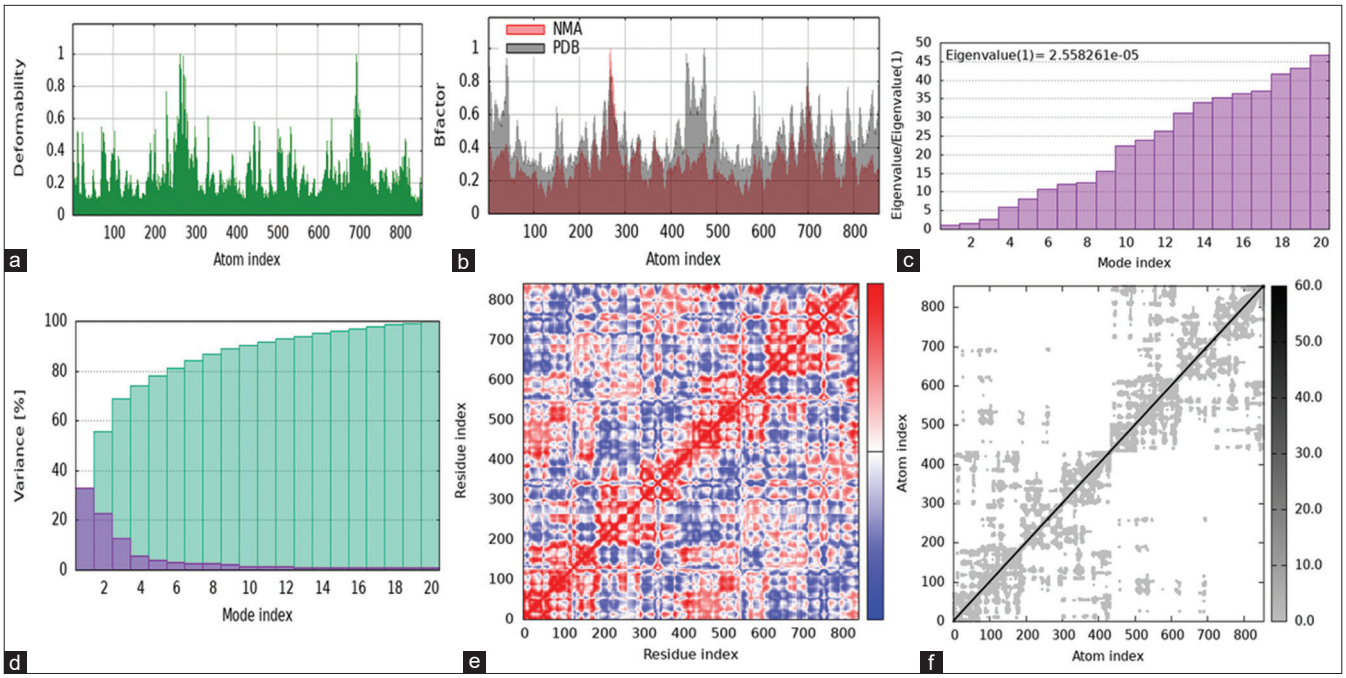

Figure 5: Normal mode analysis of the best docked compound R1 with epidermal growth factor receptor kinase complex performed using iMODS. (a) Main-chain deformability. (b) B-factor profile showing minimal mobility. (c) Eigenvalue depicting the level of deformation. (d) Variance indicating optimal stability (e) Covariance map displaying coordinated domain motion. (f) Elastic network showing strong inter-residue stiffness

Table 1: Molecular docking scores and key interacting residues of synthesised compounds (R1–R6) with EGFRK enzyme (Protein Data Bank ID: 5OEQ)

Compound	Dockscore	Interacting residues
R1	–8.1	GLN-788, GLU-762, CYS-797, VAL-726, LEU-844
R2	–7.7	ALA-743, VAL-726, ALA-751, ARG-841
R3	–7.7	ASP-855, ASN-842, ALA-743, ARG-841
R4	–7.6	GLY-719, CYS-797, VAL-726, ALA-743
R5	–7.7	GLY-719, ASP-855, ALA-743, ARG-841
R6	–7.5	GLY-719, ASP-855, PRO-794, VAL-726, ARG-841

EGFRK: Epidermal growth factor receptor kinase , GLU: Glutamate, CYS: Cysteine, VAL: Valine, LEU: Leucine, ALA: Alanine, ARG: Arginine, ASP: Aspartate, PRO: Proline, GLN: Glutamine, GLY: Glycine, ASN: Asparagine

Covariance analysis of R2 and R5 indicated well-distributed correlated motions, whereas R3 showed greater flexibility. Their elastic networks suggested moderate interaction strength and overall stability. In contrast, R4 (–7.6 kcal/moL) and R6 (–7.5 kcal/moL) displayed higher eigenvalues and lower variance, indicating reduced flexibility. R4 remained rigid with minimal deformability, while R6 showed weaker interatomic interactions and reduced cooperative motions, as reflected by a lighter elastic network. Although both formed stable complexes, their limited flexibility may affect dynamic responsiveness. Overall, R1 demonstrated the best combination of binding affinity, stability, and flexibility, followed by R2 and R5, making them suitable candidates for further studies.

In silico ADMET profiling and drug-likeness evaluation of synthesized compounds

The *in silico* ADMET profiles of six synthesised compounds (R1–R6) were evaluated using pkCSM, PreADMET, and OSIRIS to assess drug-likeness and pharmacokinetic behavior for anti-TB activity. Physicochemical, absorption, distribution, and toxicity parameters indicated favorable profiles across all compounds as shown in Tables 2-4.

All derivatives complied with Lipinski's rule of five, with molecular weights (271.31–343.40 Da), clogP (2.51–3.13), and total prostate-specific antigen values within acceptable limits, suggesting good oral bioavailability. Human intestinal absorption was high (>93%), with R1 and R5 showing the highest values. Cancer colon-2-2 and Madin-Darby Canine Kidney permeability supported efficient absorption, particularly for R1, R3, R5, and R6. BBB penetration varied, with R1 and R3 showing minimal permeability, reducing CNS-related risks, while R6 showed higher penetration. Plasma protein binding was high (>89%), with R4 exhibiting the highest value. Molecular flexibility parameters supported favorable drug–receptor interactions, especially for R1, R3, and R4.

Table 2: Physicochemical and drug-likeness properties of synthesized compounds (R1–R6)

Compound	Mol. Wt.	ClogP	Surface area	HBA	HBD	Lipin-Ski's violations	TPSA	% AB	Rotatable bonds
R1	298.32	3.13	376.34	6	1	0	115.3	92.40	3
R2	271.31	2.52	192.34	3	0	0	69.51	93.56	2
R3	343.40	2.51	381.17	7	1	0	97.26	95.79	5
R4	298.32	3.13	286.45	6	1	0	115.3	93.56	3
R5	283.35	2.65	106.46	5	1	0	78.74	95.30	3
R6	271.31	2.82	354.48	4	1	0	69.51	94.02	2

TPSA: Total prostate-specific antigen, HBA: Hydrogen bond acceptor, HBD: Hydrogen bond donor, Mol. Wt.: Molecular weight

Table 3: Predicted absorption and distribution properties of synthesized compounds (R1–R6)

Compound	MDCK	Caco-2	Human intestinal absorbance	BBB	Plasma protein binding
R1	14.272	36.919	99.29	0.016	89.5058
R2	43.786	18.567	93.67	0.568	90.6745
R3	93.633	35.286	98.80	0.010	89.8729
R4	35.347	19.459	96.78	1.4593	94.7865
R5	13.989	34.121	99.04	0.5109	91.4490
R6	96.414	27.440	98.51	3.2440	90.2721

MDCK: Madin-Darby canine kidney, Caco-2: Cancer colon-2, BBB: Blood-brain barrier

Table 4: *In silico* screening of toxicity, drug bioavailability, and drug score of synthesized compounds (R1–R6)

Compound	*In silico* screening of toxicity, drug bioavailability, and drug score
R1	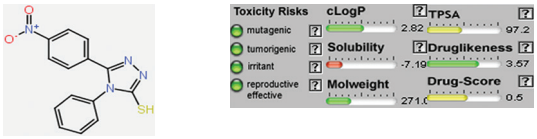
R2	
R3	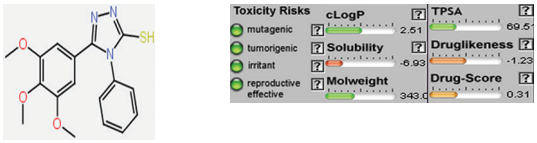
R4	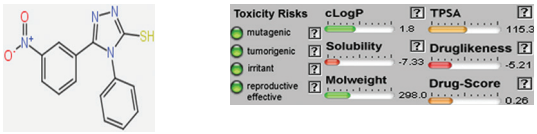
R5	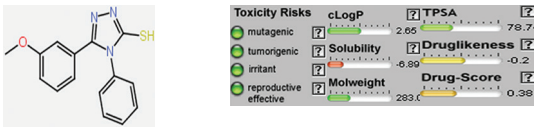
R6	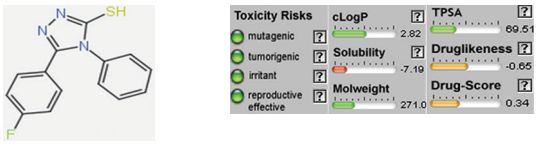

OSIRIS toxicity predictions indicated no risks of mutagenicity, tumorigenicity, irritancy, or reproductive toxicity. Overall, R3 showed optimal permeability, high absorption, minimal BBB penetration, and good safety, followed by R1 and R5. These compounds emerged as promising candidates for further biological evaluation against *M. tuberculosis*.

Anti-TB activity assessment via Alamar blue assay

The anti-mycobacterial efficacy of synthesised compounds R1–R6 was assessed against *M. tuberculosis* using the MABA, a reliable colorimetric method for determining cell viability based on redox reactions. Serial dilutions ranging from 100 µg/mL to 0.2 µg/mL were tested, with a color change from blue to pink indicating bacterial viability. The biological activity results are shown in Table 5 and Figure 6.

Compound R1 demonstrated potent activity, with a strong blue color at a MIC of 3.125 µg/ml. R2and R4 showed MIC, with the blue hue sustained down to 6.25 µg/mL. R5 and R6 showed moderate inhibition, with an MIC of 12.5 µg/mL. R3 exhibited the lowest activity with an MIC of 25 µg/mL. The positive control, the drug Rifampicin, remained blue throughout the dilution series, confirming assay reliability and showing high efficacy. The negative control (DC) turned pink, indicating full bacterial growth and appropriate assay performance. Overall, compounds R1, R2, and R4 were found to be the most promising antitubercular agents, displaying significant bacteriostatic activity at relatively low concentrations. These results align well with their favorable ADMET profiles, particularly high absorption and low BBB penetration, reinforcing their potential as lead compounds for TB treatment.

Table 5: Anti-tuberculosis activity against *Mycobacterium tuberculosis* (H_3RV) at a concentration of 100–0.2 μg/mL

Compound	Concentrations in μg/mL											
	100	50	25	12.5	6.25	3.125	1.6	0.8	0.4	0.2	PC	DC
R1	S	S	S	S	S	S	R	R	R	R	G+	NG
R2	S	S	S	S	S	R	R	R	R	R	G+	NG
R3	S	S	S	R	R	R	R	R	R	R	G+	NG
R4	S	S	S	S	S	R	R	R	R	R	G+	NG
R5	S	S	S	S	R	R	R	R	R	R	G+	NG
R6	S	S	S	S	R	R	R	R	R	R	G+	NG

PC: Positive control, DC: Drug control, S: Susceptible, R-Resistant, G+: Positive, NG: Negative

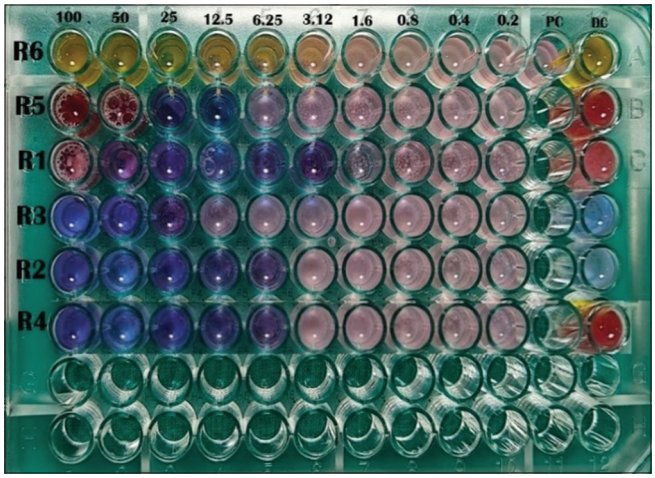

Figure 6: Antituberculosis activity of synthesized compounds (R1–R6) by the microplate Alamar Blue assay method

CONCLUSION

The present investigation reports the successful design and synthesis of a novel series of 1,2,4-triazole-3-thiol derivatives (R1–R6) aiming to develop potential anti-tubercular agents. Computational docking studies targeting EGFR kinase (PDB ID: 5OEQ) revealed favorable binding profiles for all compounds, with R1 exhibiting the strongest interaction and binding energy, supported by key hydrogen bonding and hydrophobic contacts within the active site. Structural dynamics analysis through normal mode assessment further affirmed the conformational stability of the R1-protein complex. *In silico* pharmacokinetic and toxicity evaluations demonstrated that the compounds complied with major drug-likeness filters and displayed acceptable absorption, distribution, and safety characteristics. Biological screening using the MABA confirmed significant anti-tubercular activity, particularly for R1, R2, and R4, which exhibited MIC values ranging from 12.5 to 6.25 μg/mL, respectively. Overall, integrating synthetic chemistry, computational modeling, and biological evaluation suggests that the 1,2,4-triazole-3-thiol scaffold, especially compound R1, holds considerable promise for further development as a lead structure in anti-TB drug discovery.

ACKNOWLEDGMENT

The authors are thankful to the Principal and Management Members of KLE College of Pharmacy, Vidyanagar, Hubballi, Karnataka (A Constituent College of KLE Academy of Higher Education and Research – A Deemed-to-be University, Belagavi, Karnataka, India) for providing the necessary laboratory facilities to complete the present research work at the Department of Pharmaceutical Chemistry.

REFERENCES

1. Terracciano E, Amadori F, Zaratti L, Franco E. Tuberculosis: An ever present disease but difficult to prevent. Ig Sanita Pubbl 2020;76:59-66.
2. Sandhu GK. Tuberculosis: Current situation, challenges and overview of its control programs in India. J Glob Infect Dis 2011;3:143-50.
3. Mori M, Stelitano G, Chiarelli LR, Cazzaniga G, Gelain A, Barlocco D, *et al*. Synthesis, characterization, and biological evaluation of new derivatives targeting MbtI as antitubercularagents. Pharmaceuticals (Basel) 2021;14:155.
4. Falzon D, Zignol M, Bastard M, Floyd K, Kasaeva T. The impact of the COVID-19 pandemic on the global tuberculosis epidemic. Front Immunol 2023;14:1234785.
5. Bansal R, Sharma D, Singh R. Tuberculosis and its treatment: An overview. Mini Rev Med Chem 2018;18:58-71.
6. Bendre AD, Peters PJ, Kumar J. Tuberculosis: Past, present and future of the treatment and drug discovery research. Curr Res Pharmacol Drug Discov 2021;2:100037.
7. Seung KJ, Keshavjee S, Rich ML. Multidrug-resistant tuberculosis and extensively drug-resistant tuberculosis. Cold Spring Harb Perspect Med 2015;5:a017863.
8. Lohiya A, Suliankatchi Abdulkader R, Rath RS, Jacob O, Chinnakali P, Goel AD, *et al*. Prevalence and patterns of drug resistant pulmonary tuberculosis in India-A systematic review and meta-analysis. J Glob Antimicrob Resist 2020;22:308-16.

9. Migliori GB, Sotgiu G, D'Arcy Richardson M, Centis R, Facchini A, Guenther G, *et al*. MDR-TB and XDR-TB: Drug resistance and treatment outcomes. Eur Respir J 2009;34:778-9.
10. Nataraj V, Varela C, Javid A, Singh A, Besra GS, Bhatt A. Mycolic acids: Deciphering and targeting the A chilles' heel of the tubercle Bacillus. Molmicrobiol 2015;98:7-16.
11. Fil M, Alibert S. Unveiling DprE1 as a key target in the fight against tuberculosis: Insights and perspectives on developing novel antimicrobial agents. BioMed 2024;4:220-36.
12. Manina G, Pasca MR, Buroni S, De Rossi E, Riccardi G. Decaprenylphosphoryl-β-D-ribose 2'-epimerase from *Mycobacterium tuberculosis* is a magic drug target. Curr Med Chem 2010;17:3099-108.
13. Brecik M, Centarova I, Mukherjee R, Kolly GS, Huszár S, Bobovská A, *et al*. DprE1 is a vulnerable tuberculosis drug target due to its cell wall localization. ACS Chem Bio 2015;10:1631-6.
14. Zhang S, Xu Z, Gao C, Ren QC, Chang L, Lv ZS, *et al*. Triazole derivatives and their anti-tubercular activity. Eur J Med Chem 2017;138:501-13.
15. Havaldar FH, Patil AR. Syntheses of 1, 2, 4 triazole derivatives and their biological activity. J Chem 2008;5:347-54.
16. Gupta O, Pradhan T, Chawla G. An updated review on a diverse range of biological activities of 1, 2, 4-triazole derivatives: Insight into structure-activity relationship. J Mol Struct 2023;1274:134487.
17. Gupta D, Jain DK. Synthesis, antifungal and antibacterial activity of novel 1,2,4-triazole derivatives. J Adv Pharm Technol Res 2015;6:141-6.
18. Karabanovich G, Roh J, Smutna T, Nemecek J, Vavrova K, Huszar S, *et al*. 1,2,4-triazole-3-thiol derivatives with anti-mycobacterial activity. Eur J Med Chem 2019;181:111589.
19. Briki K, Lahreche T, Abbassi MS, Lahrech MB, Othman AA, Elissawy AM, *et al*. Benzohydrazide as a good precursor for the synthesis of novel bioactive and anti-oxidant 2-phenyl-1,3,4-oxadiazol-aminoacid derivatives: Structural determination, biological and anti-oxidant activity. Arab J Chem 2024;17:105767.
20. Bayrak H, Demirbas A, Karaoglu SA, Demirbas N. Synthesis of some new 1,2,4-triazoles, their Mannich and schiff bases and evaluation of their antimicrobial activities. Eur J Med Chem 2009;44:1057-66.
21. Dave AY, Parmar KA, Begari E, Joshi DS. Synthesis and biological evaluation of oxadiazole clubbed thiadiazole derivatives as antimicrobial agents. Indian J Heterocycl Chem 2021;31:273-80.
22. Laskowski RA, MacArthur MW, Moss DS, Thornton JM. PROCHECK: A program to check the stereochemical quality of protein structures. J Appl Crystallogr 1993;26:283-91.
23. Laskowski RA, Rullmannn JA, MacArthur MW, Kaptein R, Thornton JM. AQUA and PROCHECK-NMR: Programs for checking the quality of protein structures solved by NMR. J Biomol NMR 1996;8:477-86.
24. Lohning AE, Levonis SM, Williams-Noonan B, Schweiker SS. A practical guide to molecular docking and homology modelling for medicinal chemists. Curr Top Med Chem 2017;17:2023-40.
25. Kitchen DB, Decornez H, Furr JR, Bajorath J. Docking and scoring in virtual screening for drug discovery: Methods and applications. Nat Rev Drug Discov 2004;3:935-49.
26. Özkul Ş, Tunca E, Mert S, Bayrakdar A, Kasımoğulları R. Synthesis, molecular docking analysis, drug-likeness evaluation, and inhibition potency of new pyrazole-3,4-dicarboxamides incorporating sulfonamide moiety as carbonic anhydrase inhibitors. J Biochem Mol Toxicol 2024;38:e23704.
27. López-Blanco JR, Aliaga JI, Quintana-Ortí ES, Chacón P. iMODS: Internal coordinates normal mode analysis server. Nucleic Acids Res 2014;42:W271-6.
28. Lopéz-Blanco JR, Garzón JI, Chacón P. iMod: Multipurpose normal mode analysis in internal coordinates. Bioinformatics 2011;27:2843-50.
29. Alsedfy MY, Ebnalwaled AA, Moustafa M, Said AH. Investigating the binding affinity, molecular dynamics, and ADMET properties of curcumin-IONPs as a mucoadhesive bioavailable oral treatment for iron deficiency anemia. Sci Rep 2024;14:22027.
30. Wu F, Zhou Y, Li L, Shen X, Chen G, Wang X, *et al*. Computational approaches in preclinical studies on drug discovery and development. Front Chem 2020;8:726.
31. Ferreira LL, Andricopulo AD. ADMET modeling approaches in drug discovery. Drug Discov Today 2019;24:1157-65.
32. Pires DE, Blundell TL, Ascher DB. pkCSM: Predicting small-molecule pharmacokinetic and toxicity properties using graph-based signatures. J Med Chem 2015;58:4066-72.
33. Sander T, Freyss J, Von Korff M, Reich JR, Rufener C. OSIRIS, an entirely in-house developed drug discovery informatics system. J Chem Inf Model 2009;49:232-46.
34. Banerjee P, Kemmler E, Dunkel M, Preissner R. ProTox 3.0: A webserver for the prediction of toxicity of chemicals. Nucleic Acids Res 2024;52:W513-20.
35. Banerjee P, Eckert AO, Schrey AK, Preissner R. ProTox-II: A webserver for the prediction of toxicity of chemicals. Nucleic Acids Res 2018;46:W257-63.
36. Modi P, Patel S, Chhabria M. Structure-based design, synthesis and biological evaluation of a newer series of pyrazolo[1,5-a]pyrimidine analogues as potential anti-tubercular agents. Bioorg Chem 2019;87:240-51.

Source of Support: Nil. **Conflicts of Interest:** None declared.